Revista Mexicana de Astronomía y Astrofísica, **49**, 227–238 (2013)

THE LATEST ERUPTION OF PLANETARY NEBULA IC 2165[1]

J. Bohigas,[2] M. Rodríguez,[3] and R. J. Dufour[4]

Received 2013 January 17; accepted 2013 April 15

RESUMEN

Espectroscopía de alta dispersión con rendija abierta de la región interna de la nebulosa planetaria (NP) IC 2165, revela que su temperatura es elevada y relativamente uniforme, mientras que la densidad es mucho mayor cerca del núcleo de la NP. Las abundancias indican que no es una NP de tipo I. Una gran cantidad de calcio y hierro está atrapada en granos. La masa ionizada es al menos $\sim$0.05 $M_\odot$. Un modelo de fotoionización (CLOUDY, version 10.00) que supone una ley del cuadrado inverso para la densidad y abundancias típicas de NP que no son de tipo I, reproduce razonablemente bien el espectro y los cocientes de líneas sensibles a densidad y temperatura, pero no las propiedades globales de la NP. Todo indica que IC 2165 fue producida por una estrella A5 V de 2 $M_\odot$ y pobre en metales, que arrancó hace unos 2×10^9 años.

ABSTRACT

Open slit high dispersion spectroscopic observations of the inner region of planetary nebula (PN) IC 2165 indicate that the object has a relatively uniform and high electron temperature, with its density being much larger close to the PN nucleus. Abundances imply that it is a non-type I PN. Calcium and iron have been heavily depleted into grains. The ionized mass is at least $\sim$0.05 $M_\odot$. A photoionization model (CLOUDY, version 10.00) assuming an inverse square law for the density and abundances typical of a non-type I PN, produced a fair replica of the spectrum and of all electron density and temperature sensitive line ratios, but not of the global properties of this object. All evidence indicates that IC 2165 was produced by a metal poor 2 $M_\odot$ A5 V star that took off some 2×10^9 yr ago.

Key Words: planetary nebulae: general — ISM: abundances — ISM: individual (IC 2165)

1. INTRODUCTION

Planetary nebula (PN) IC 2165 (G 221.3-12.3) is composed of two faint halos located 20″ and 33″ from the central star (Corradi et al. 2003) and a bright nearly circular $\sim$10″ nebula at the center (Tylenda et al. 2003). Acker et al. (2002) determined that the inner nebula is expanding uniformly at 25 km s^{-1} and found turbulence with a characteristic velocity of 14 km s^{-1}. IC 2165 is thought to be between 1.1 and 3.9 kpc away from us, and the mean distance estimate is 2.53 ± 0.80 kpc (Daub 1982; Maciel 1984; Cahn, Kaler, & Stanghellini 1992; Van de Steene & Zijlstra 1994; Zhang 1995; Tajitsu & Tamura 1998; Phillips 2004; Stanghellini, Shaw, & Villaver 2008), which implies that it is at 539 ± 17 pc from the galactic plane. The radial velocity is between 55.3 and 50 km s^{-1} (Campbell & Moore 1918; Wilson 1950), which corresponds to a Local Standard of Rest radial velocity between 35 and 40 km s^{-1} when using the basic solar motion parameters provided by Mihalas & Binney (1981). The central star has been classified as a weak emission line star (Acker & Neiner 2003). Using HST images and assuming that the central star is a 200,000°K black body, Wolff, Code, & Groth (2000) determined that $E(B-V) = 0.40$, $B = 17.50 \pm 0.06$ and $V = 17.47 \pm 0.06$. The visual magnitude and temperature may be too large, since Heap et al. (1990)

[1]Based on observations collected at the Observatorio Astronómico Nacional in San Pedro Mártir, B. C., Mexico.

[2]Instituto de Astronomía, Universidad Nacional Autónoma de México, Ensenada, B. C., Mexico.

[3]Instituto Nacional de Astrofísica, Óptica y Electrónica, Puebla, Pue., Mexico.

[3]Rice University, USA.

found that the central star Zanstra temperature is $150,000$°K and $V = 16.93$.

Using a dual photoelectric spectral scanner with a 16.4–32.8 Å/mm dispersion and an 18.″2 circular aperture, Gutiérrez-Moreno, Moreno, & Cortés (1985, henceforth GMC) obtained emission line fluxes from 3400 to 7330 Å of the whole innermost region of IC 2165. Later on, Kwitter, Henry, & Milingo (2003, henceforth KHM) covered a larger spectral range (3700 to 9600 Å) with a lower dispersion (100–127 Å/mm) and a $5'' \times 285''$ entrance slit that did not include the entire inner region. High dispersion (1.3–3.2 Å/mm) optical Echelle spectroscopy from ∼3400 to 10200 Å, was produced by Hyung (1994, henceforth H94) using a 1.″16 wide and $4''$ long entrance slit. Several positions for the CCD chip were required to cover the entire spectrum. On the other hand, Pottasch et al. (2004) collected mid-infrared ISO observations of IC 2165, with apertures large enough to include the entire innermost nebula and both halos at the longest wavelengths (from $14'' \times 20''$ below 12 μm and $80''$ beyond 45 μm). Finally, H94 and Pottasch et al. (2004) also include a selection of spectra taken by the IUE satellite with a $10'' \times 23''$ entrance aperture. From all this, Quireza, Rocha-Pinto, & Maciel (2007) conclude that IC 2165 is a Peimbert type IIb PN.

Based on long exposure high dispersion optical spectroscopic observations of the entire innermost nebula, this paper re-analyzes what may be latest eruption of IC 2165. With this instrumental setup we can sample the entire photoionized region and develop a meaningful photoionization model, something that can be problematic with narrow slit observations, and, as opposed to low dispersion spectroscopy, meaningful data are not lost due to line blending. Observations are described in § 2. Standard procedures are used to reduce and analyze the data and obtain densities, temperatures, a large number of ion concentrations, abundances and the ionized gas mass, as described in § 3. In § 4 the spectrum is modeled using the Cloudy photoionization code, thus providing an additional estimate of nebular abundances as well as important insights on the physical structure of the innermost nebula and on the properties and origin of the exciting star. Conclusions are presented in the final section.

2. OBSERVATIONS

Spectroscopy was carried out on January 2011, using the 2.1 m f/7.5 telescope at OAN, and the Echelle spectrograph with a 400 lines mm^{-1} cross disperser, no blocking filters and a 1.7 mm wide and 2.0 mm long slit (∼$22'' \times 27''$). The slit was fully open in order to minimize problems related to incomplete coverage and to capture all the emission produced by the inner nebula (Bohigas 2008). The position of the slit in relation to IC 2165 is depicted in Figure 1. The detector was a Thomson 2048×2048 pixel CCD, binned by a factor of two in both directions.

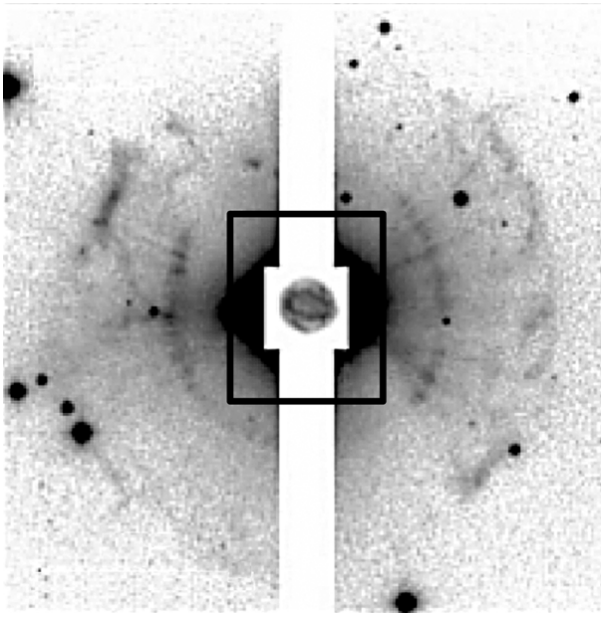

Fig. 1. Entrance slit ($22'' \times 27''$ black frame) on an Hα+[N II] image from Corradi et al. (2003).

The spectral range, mean spectral resolution and dispersion are $\lambda\lambda$3650-6700 Å, ∼2.5 pixel and between 0.28 (red end) and 0.16 (blue end) Å/pixel. Since the binned pixel size is 30 μm, the dispersion is between 5.3 and 9.3 Å/mm. The spectrum used for the brightest lines was obtained combining 5 exposures, each 120 s long. For the other lines, the spectrum was extracted from an image combining 12 exposures, each 600 s long. Data reduction was performed applying IRAF[5] standard procedures.

The results are reported in Table 1. Line fluxes were determined using standard stars HR 1544 and HR 3544 (16 Å data bins) with and without background subtraction. Notice that the background includes part of the much fainter halos. Mean fluxes relative to Hβ, along with the largest deviation for these measurements, are given under the column labeled as $F_{\rm obs}$. These deviations yield a rough estimate of measurement errors, since most line fluxes were quantified at least four times: two standards,

[5]IRAF is distributed by NOAO which is operated by AURA under contract to the NSF.

TABLE 1

IC 2165 SPECTRUM[a]

ID	F_{obs}	I_{obs}	I_{mod}	ID	F_{obs}	I_{obs}	I_{mod}
[O II] 3726	21.90 ± 1.34	27.82	26.06	[O III] 4931	0.21 ± 0.03	0.21	0.16
[O II] 3729	13.10 ± 0.73	16.63	17.41	[O III] 4959	426.00 ± 3.83	417.29	389.67
H 13 3734	1.10	1.39	2.72	[O III] 5007	1300.00 ± 14.30	1260.91	1172.90
H 12 3750	2.14	2.70	3.28	He I 5016	1.12 ± 0.13	1.08	2.35
O III 3760	2.39	3.01	0.17	He I 5048	0.12	0.12	0.20
H 11 3771	2.93	3.68	4.10	[Fe VI] 5146	0.10 ± 0.03	0.10	···
H 10+He II 3798	3.55 ± 0.31	4.43	5.55	[Fe VII] 5159	0.07	0.07	0.03
H 9+He II 3835	5.26 ± 0.08	6.50	7.53	[Fe VI] 5176	0.06	0.06	0.05
[Ne III]+He I 3869	66.30 ± 5.11	81.36	81.88	[Ar III] 5192	0.20 ± 0.06	0.19	0.12
H 8+He I+He II 3889	17.00 ± 1.48	20.77	14.58	[N I] 5198	0.34 ± 0.04	0.32	0.07
[Ne III] 3968	28.80 ± 4.52	34.57	24.68	[N I] 5200	0.22 ± 0.05	0.21	0.05
Hϵ+He II 3970	15.50 ± 3.32	18.59	16.37	[Fe III] 5270	0.05	0.05	0.03
He I+He II 4026	1.91 ± 0.41	2.26	2.23	[Ca V]+[Fe III] 5309	0.06	0.06	0.05
[S II] 4069	1.12 ± 0.12	1.32	1.35	[Cl IV] 5323	0.06	0.05	0.02
C III 4070	0.35 ± 0.07	0.41	0.56	[Fe VI] 5335	0.07	0.06	···
[S II]+O II 4076	0.40 ± 0.08	0.47	0.56	[Kr IV] 5345	0.09	0.08	···
N III 4097	1.82 ± 0.49	2.13	···	He II 5412	4.12 ± 0.06	3.72	3.17
Hδ+He II 4101	22.90 ± 2.18	26.72	26.70	[Cl III] 5518	0.52 ± 0.05	0.46	0.49
He I 4121	0.29	0.34	0.24	[Cl III] 5538	0.64 ± 0.02	0.56	0.59
He I 4144	0.23 ± 0.03	0.27	0.30	[O I] 5577	2.08	1.81	0.01
He II 4200	0.68 ± 0.02	0.78	0.75	O III 5592	0.07 ± 0.01	0.06	···
[Fe V] 4227	0.12	0.14	···	[Fe VII] 5721	0.06	0.05	0.06
C II 4267	0.30	0.34	0.33	[N II] 5755	1.52 ± 0.02	1.28	1.34
He II 4339	1.33	1.49	1.00	C IV 5802	0.23 ± 0.01	0.19	···
Hγ 4340	43.50 ± 1.91	48.84	47.26	C IV 5812	0.12	0.10	···
[O III] 4363	18.60 ± 0.54	20.79	19.13	[Kr IV] 5868	0.14 ± 0.02	0.12	···
He I 4388	0.37 ± 0.01	0.41	0.47	He I 5876	14.50 ± 0.14	11.94	12.31
He I 4471	3.37 ± 0.05	3.67	3.86	He II 5882	0.06	0.05	···
He II 4542	1.44 ± 0.04	1.54	1.40	Na I 5889	0.29	0.24	···
[Mg I] I 4563	0.06	0.06	···	Na I 5895	0.13	0.11	···
Mg I 4571	0.23 ± 0.01	0.24	···	He II 5913	0.14	0.11	···
N III 4634	0.88 ± 0.04	0.92	···	He II 5932	0.13	0.11	···
N III 4641	2.08 ± 0.09	2.18	···	He II 5977	0.12	0.10	···
C III 4647	0.26 ± 0.01	0.27	···	He II 6005	0.08	0.06	···
O II 4649	0.05 ± 0.01	0.05	0.21[b]	He II 6037	0.10	0.08	···
C III 4650	0.15 ± 0.01	0.16	0.53[c]	He II 6074	0.12	0.10	0.11
C III+O II 4651	0.07 ± 0.04	0.07	···	[Fe VII]+[Ca V] 6087	0.11	0.09	0.09
C IV+[Fe III] 4659	0.44 ± 0.01	0.42	0.43	[K IV] 6102	0.35 ± 0.01	0.28	···
O II 4662	0.05	0.05	···	He II 6118	0.18 ± 0.03	0.14	0.12
He II 4686	41.20 ± 0.66	42.75	0.90	He II 6171	0.16 ± 0.02	0.13	0.13
O II 4699	0.34	0.35	···	He II 6234	0.27 ± 0.05	0.21	0.15
[Fe III] 4702	0.21	0.22	0.02	[O I] 6300	4.46	3.45	0.48
[Ar IV] 4711	4.16 ± 0.14	4.30	3.80	[S III]+He II 6312	2.80 ± 0.05	2.16	2.41
He I 4713	0.68 ± 0.02	0.70	0.76	[O I] 6364	1.42	1.09	0.22
[Ne IV] 4715	0.49 ± 0.05	0.51	···	He II 6406	0.32 ± 0.01	0.24	0.15
[Ne IV] 4717	0.13 ± 0.06	0.13	0.58[d]	[Ar V] 6435	0.81 ± 0.01	0.62	1.15
[Ne IV] 4725	0.46 ± 0.04	0.47	···	He II 6527	0.32 ± 0.01	0.24	0.23
[Ne IV] 4727	0.36 ± 0.13	0.37	···	[N II] 6548	20.80 ± 0.15	15.59	16.34
[Ar IV] 4740	5.08 ± 0.13	5.20	5.95	He II 6560	11.20 ± 3.08	8.38	5.44
He II 4859	2.64 ± 0.40	2.64	2.04	Hα 6563	446.00 ± 3.57	333.71	280.51
Hβ 4860	100.00	100.00	100.00	C II 6578	0.12 ± 0.03	0.09	0.04
He I 4922	0.90 ± 0.07	0.89	1.03	[N II] 6584	67.00 ± 0.54	50.04	48.22

[a] $F(H\beta)=1.31\pm0.05\times10^{-11}$ erg cm^{-2} s^{-1}; $C(H\beta)=0.39$; $I(H\beta)=3.22\pm0.12\times10^{-11}$ erg cm^{-2} s^{-1}.
[b] Sum of the intensities of O II 4649, 4651 and 4662.
[c] Sum of the intensities of C III 4647, 4650 and 4651.
[d] Sum of the intensities of [Ne IV] 4715, 4717, 4725 and 4727.

with and without background subtraction and, in some cases, the line could be measured in two spectral orders. For obvious reasons, deviations are not given for some weak and all atmospheric lines, which could not be measured more than twice. In this case, uncertainties may be as large as ∼50%. Draw-

TABLE 2

DENSITIES AND TEMPERATURES

Line ratio	Value	N_e (cm^{-3})
[N I]5198/5200	$1.52^{+0.69}_{-0.44}$	1072^{+4417}_{-731}
[O II]3726/3729	$1.67^{+0.21}_{-0.19}$	1589^{+519}_{-390}
[Cl III]5518/5538	$0.82^{+0.12}_{-0.11}$	5251^{+2894}_{-1951}
[Ar IV]4711/4740	$0.83^{+0.05}_{-0.05}$	8541^{+1399}_{-1270}
Line ratio	**Value**	**T_e (°K)**
[O I](6300+6364)/5577	2.51	INDEF
[N II](6548+6584)/5755	$51.27^{+1.13}_{-1.10}$	13259^{+145}_{-142}
[O III](4959+5007)/4363	$80.72^{+3.42}_{-3.27}$	13954^{+226}_{-218}

ing a comparison between the theoretical and de-reddened values of line ratios [O III] 5007/4959 and [N II] 6584/6548, it can be argued that the minimum error level is ∼5%.

Finally, the FWHM of the Hα emission line is ∼5.″1, which indicates that the entire innermost brightest region of IC 2165 has been included in the entrance slit, since the nebular diameter at the 10% level of peak surface brightness of the Hα + [N II] (6548+6584) image is 9.″0×8.″9 (Tylenda et al. 2003). Notice that GMC observed the entire inner nebula, KHM covered approximately half of it and H94 sampled a much smaller region.

Since PNe may have two components with very different temperatures, it is sensible to determine C(Hβ) using the Balmer line ratio with the weakest density and temperature dependence, I(Hγ)/I(Hβ). For densities smaller than 10^6 cm^{-3} and temperatures between 3000 and 15000 K, the mean case B value of this Balmer line ratio is 0.467 ± 0.008 (Storey & Hummer 1995). Using Seaton's (1979) extinction law and assuming that I(Hγ)/I(Hβ)=0.467, C(Hβ)=0.24, which is markedly smaller than previous estimates (0.51, GMC; 0.68, H94; 0.40, KHM 2003), as well as the value it would take assuming that I(Hα)/I(Hβ)=2.85 (0.60).

Alternatively, C(Hβ) can be selected from the best fit between a set of de-reddened and theoretical Balmer line ratios. To do so we use Hα, Hγ, Hδ, Hϵ and H9 over Hβ, the brightest Balmer lines that are not greatly affected by blending. A weight factor proportional to the measurement errors given in Table 1 is assigned to each line: 0.7 for errors between 20% and 30%, 0.8 if these are larger than 10%, 0.9 when they exceed 5% and 1 when they are smaller than this. Since Balmer line ratios depend on the electron density and temperature, we assume that the former is equal to 10000 cm^{-3}, as implied by our observations (see Table 2) and, for a given temperature T(H$^+$), determine which is the value of C(Hβ) that minimizes the difference between observed and theoretical Balmer line ratios. Doing so, best fits were found for C(Hβ)=0.24, 0.32, 0.39, 0.44 and 0.47, when T(H$^+$)=1000, 2500, 5000, 10000 and 15000°K. Among these, the optimal combination is for C(Hβ)=0.39 and T(H$^+$)=5000°K. Since T(H$^+$) is the temperature at which Balmer recombination lines are produced, this suggests that there may be a colder component where recombination lines are important cooling agents, in addition to the hot gas where forbidden line emission is mostly produced. De-reddened line fluxes appearing under the label $I_{\rm obs}$ in Table 1, were computed assuming that C(Hβ)=0.39. Line fluxes from the photoionization model that is discussed in § 4, are included in this table under the column labeled $I_{\rm mod}$.

3. DATA ANALYSIS

3.1. *Nebular densities and temperatures*

Electron densities and temperatures are shown in Table 2. These were calculated using IRAF's TEMDEN task (Shaw & Dufour 1994). Assuming that O$^+$ and N$^+$ coexist in the same nebular region, solutions for the electron temperature and density, T_e(N$^+$) = 13259°K and N_e(O$^+$) = 1589 cm^{-3}, were obtained self-consistently from [N II](6548+6584)/5755 and [O II]3726/3729. The electron density found from the [N I]5198/5200, N_e(N^0 =1072 cm^{-3}, was determined assuming that T_e(N$^+$) is the electron temperature in the N^0 region. Likewise, assuming that O^{+2} and Ar^{+3} coexist in the same nebular region, solutions for the electron temperature and density, T_e(O^{+2}) = 13954°K and N_e(Ar^{+3}) = 8541 cm^{-3}, were obtained self-consistently from [O III](4959+5007)/4363 and [Ar IV]4711/4740. The electron density found from the [Cl III]5518/5538, N_e(Cl^{+2}) = 5251 cm^{-3}, was determined assuming that the electron temperature in the Cl^{+2} region is the average of T_e(N$^+$) and T_e(O^{+2}). An estimate of the electron temperature in the neutral region could not be found from [O I](6300+6364)/5577, because of deficient sky subtraction in the intrinsically very faint [O I] 5577 Å line.

In order to make a meaningful comparison with other works, we applied IRAF's TEMDEN package to previously reported line ratios. From these ratios we derive similar values for the electron temperature and density of the highly excited region of

the nebula: $T_e(O^{+2}) \simeq 13800$, 13700 and 14600°K and $N_e(Ar^{+3}) \simeq 6800$, 3700 and 6800 cm^{-3} (GMC, KHM and H94 respectively). We also obtain similar numbers for $N_e(O^+)$ and $N_e(N^0)$ from line ratios reported by H94 (2400 and 900 cm^{-3}). Our nitrogen temperature, $T_e(N^+)$, is quite similar to those derived from the data presented by KHM (14400°K) and H94 (13400°K), but substantially larger than the one obtained from the GMC line ratio (9300°K). Rather surprisingly, the [S II]6717/6731 line ratio reported by GMC, KHM and H94 (not measured by us) leads to electron densities between 3300 and 6300 cm^{-3}, substantially larger than $N_e(O^+)$ and $N_e(N^0)$.

Thus, temperature in the inner nebula appears to be large and, by most accounts, roughly uniform. This large temperature implies that the vigorous turbulence found by Acker et al. (2002) is subsonic, as it should be. The photoionization model supports this observation. On the other hand, the density is somewhat larger, much larger according to H94 and our data, in the highly ionized regions which are closer to the central star. Consequently, thermal pressure is driving part of the expansion of the innermost region of IC 2165.

3.2. *Nebular abundances from ionization correction factors*

Ion abundances are given in Table 3. IRAF's IONIC task (Shaw & Dufour 1994) was used to determine forbidden line abundances for most ions. The concentration of helium ions was calculated following Aller (1984), taking into account collisional effects on the He I lines (Kingdon & Ferland 1995).

Case A effective recombination coefficients from Davey, Storey, & Kisielius (2000), Péquignot, Petitjean, & Boisson (1991) and Storey (1994) were used to determine the abundances of C^{+2} from C II 4267, C^{+3} from the C III 4070 Å line and the multiplet at 4647, 4650 and 4651 Å, and O^{+2} from the O II 4649, 4651 and 4662 Å multiplet. We assume that the intensity of the line blend at 4651 Å, which accounts for less than 30% of the total flux of both multiplets, is equally divided by the C III and O II lines. The abundance of C^{+4} can not be estimated since C IV 4659 is blended with an [Fe III] line and, as far as we know, the effective recombination coefficients for C IV 5802 and 5812Å are not available. Notice that O III 3760 and 5592 Å, as well as N III 4097, 4634 and 4641 Å, cannot be used to find the concentrations of O^{+3} and N^{+3} since these lines are produced by the Bowen fluorescence mechanism (Grandi 1976).

TABLE 3

ION CONCENTRATIONS

Ion	Line	Std	2C
He^+	5876	0.071	0.075
He^{+2}	4686	0.047	0.060
C^{+2} $\times10^{-4}$	4267	3.56	2.91
C^{+3} $\times10^{-4}$	4070	2.72	2.10
C^{+3} $\times10^{-4}$	4650	3.79	5.18
N^0 $\times10^{-7}$	5198	1.81	4.18
N^+ $\times10^{-6}$	6584	5.09	11.8
O^0 $\times10^{-6}$	6300	2.51	5.80
O^+ $\times10^{-6}$	3727	7.22	16.7
O^{+2} $\times10^{-4}$	5007	1.42	3.44
O^{+2} $\times10^{-4}$	4649	1.08	1.18
Ne^{+2} $\times10^{-5}$	3869	2.52	5.45
Ne^{+3} $\times10^{-5}$	4720[a]	2.44	6.29
S^+ $\times10^{-7}$	4069	1.38	3.19
S^{+2} $\times10^{-6}$	6312	1.58	3.74
Cl^{+2} $\times10^{-8}$	5528[b]	3.18	7.52
Cl^{+3} $\times10^{-8}$	5323	3.19	7.72
Ar^{+2} $\times10^{-7}$	5192	6.05	14.3
Ar^{+3} $\times10^{-7}$	4740	3.86	9.34
Ar^{+4} $\times10^{-7}$	6435	1.24	3.20
K^{+3} $\times10^{-8}$	6102	1.09	2.64
Ca^{+4} $\times10^{-9}$	5309	4.04	10.4
Fe^{+2} $\times10^{-8}$	4702	14.7	33.2
Fe^{+2} $\times10^{-8}$	5270	2.11	4.77
Fe^{+4} $\times10^{-8}$	4227	2.59	6.14
Fe^{+5} $\times10^{-8}$	5146	2.39	6.04
Fe^{+5} $\times10^{-8}$	5176	1.56	3.94
Fe^{+5} $\times10^{-8}$	5335	3.40	8.60
Fe^{+6} $\times10^{-8}$	5721	1.24	3.14
Kr^{+3} $\times10^{-9}$	5868	2.19	5.64

[a]From [Ne IV]4715 + [Ne IV]4717 + [Ne IV]4725 + [Ne IV]4727.

[b]From [Cl III]5518 + [Cl III]5538.

The abundance of Fe^{+2} was calculated by solving the equations of statistical equilibrium for 34 energy levels using the transition probabilities of Quinet (1996) and the collision strengths of Zhang (1996). For Fe^{+4} we used a 34-level atom with transition probabilities from Nahar et al. (2000) and collision strengths from Ballance, Griffin, & McLaughlin (2007). For Fe^{+5} we used a 19-level atom with transition probabilities and collision strengths from

Chen & Pradhan (1999, 2000). For Fe^{+6} we used a 9-level atom with transition probabilities and collision strengths from Witthoeft & Badnell (2008).

The abundance of Kr^{+3} was determined with a five level atom model using experimental energy levels listed by NIST, transition probabilities from Biémont & Hansen (1986) and effective collision strengths from Schöning (1997).

Ion concentrations were calculated assuming the following combinations for the electron temperature and density: $T_e(N^+)$ and $N_e(O^+)$ for N^0, N^+, O^0, O^+ S^+ and Fe^{+2}, the average of $T_e(N^+)$ and $T_e(O^{+2})$ and $N_e(Cl^{+2})$ for He^+, S^{+2}, Cl^{+2} and Ar^{+2}, $T_e(O^{+2})$ and $N_e(Ar^{+3})$ for He^{+2}, C^{+2}, O^{+2}, Ne^{+2}, Cl^{+3}, Ar^{+3}, K^{+3} and Fe^{+4} and $T_e(O^{+2})$ +1000 and $N_e(Ar^{+3})$ for C^{+3}, Ne^{+3}, Ar^{+4}, Ca^{+4}, Fe^{+5}, Fe^{+6} and Kr^{+3}.

In the standard approach (under header Std in Table 3), concentrations relative to H^+ are calculated assuming that the temperature of ionized hydrogen is equal to the temperature of the ion whose abundance is to be determined. Since there can only be one mean temperature for ionized hydrogen, this often used procedure is clearly inconsistent and prone to errors, though these will not be larger than ∼15% as long as the temperature is between 9000 and 15000°K.

But the standard approach can no longer be used if there is a colder component, since the emissivity of Balmer lines is greater at lower temperatures, whereas forbidden lines are much weaker. Thus, the weighed mean temperature of the region where hydrogen recombination lines are emitted is substantially different from the mean temperature of the region where most of the emission from forbidden lines is produced. Ion concentrations given under header 2C in Table 3, were calculated using the aforementioned temperatures for forbidden lines, but assuming that the weighted temperature for all recombination lines, including those produced by hydrogen and helium, is $T(H^+) = 5000$°K, the one where the difference between observed and theoretical Balmer line ratios is smaller.

As expected, ion concentrations derived from collisionally excited lines are larger when hydrogen Balmer line emission is produced in a a colder medium. Finally, 2C abundances will be somewhat smaller when forbidden line emission in the cold component is taken into account and if the electron density is larger in the cold gas.

Chemical abundances were calculated from the ionization correction factors (ICF) for O, Ne, S, Ar and Cl given by Kingsburgh & Barlow (1994). In the case of oxygen, we used the O^{+2} abundance from [O III] 5007 Å, though the abundance found from the O II 4649 multiplet is not too different. In the case of carbon, we simply added the abundance of C^{+2} to the mean value of the C^{+3} abundances given in Table 3. There is no obvious correction to include C^+ and C^{+4}, but their significance is probably secondary. The total iron abundance was determined by adding up the contributions of all observed ions, excepting Fe^+, and assuming that Fe^{+3} has an abundance intermediate between those derived for Fe^{+2} and Fe^{+4}. We excluded Fe^+ from the abundance determination because the observed [Fe II] line is probably affected by fluorescence effects (Verner et al. 2000) and the import of Fe^+ can be considered negligible for this high excitation object (see Delgado-Inglada et al. 2009). For Fe^{+2} we adopted the mean abundance derived from the two [Fe III] lines. In the case of Fe^{+5} we adopted the average value, since the three [Fe VI] lines have a similar intensity. To the best of our knowledge there are no ICF's for K^{+3}, Ca^{+4} and Kr^{+3}. Based on similarities of atomic numbers and ionization potentials, we provide a rough estimate for the abundance of these elements using the following relationships:

$$\mathrm{K/Ar} = \mathrm{K^{+3}/Ar^{+3}}, \quad (1)$$

$$\mathrm{Ca/Ar} = \mathrm{Ca^{+4}/Ar^{+4}}, \quad (2)$$

$$\mathrm{Kr/Ar} = \mathrm{Kr^{+3}/Ar^{+3}}, \quad (3)$$

Since the ionization potentials of the first five ionization stages of krypton are similar to the first four ionization stages of argon, equation 3 probably is an adequate approximation to the abundance of Kr in IC 2165, where nearly all important argon ion abundances can be estimated. This is not as clear for potassium and calcium, but model results indicate that all these approximations are reasonable (see § 4).

Chemical abundances based on ICFs are presented in Table 4 under headers Std and 2C. In this table we also also include abundances from the best photoionization model discussed in § 4, and those reported by KHM and H94 (ICF method). Under header PN, we include mean He, C, N, O, Ne, Ar and Cl abundances for non-type I PN (Kingsburgh & Barlow 1994; Peimbert, Luridiana, & Torres-Peimbert 1995; Henry, Kwitter, & Bates 2000; Sterling, Dinerstein, & Kallman 2007; Bohigas 2008), the range of iron abundances of 24 Galactic PNe (Delgado-Inglada et al. 2009) and the mean krypton abundance of 10 more (Sterling et al. 2007). The last column is the average of solar abundances

TABLE 4

CHEMICAL ABUNDANCES

Element	Std	2C	Model	KHM	H94	PN	Solar
He	0.118	0.135	0.106	0.09	0.107	0.111 ± 0.020	0.082
C $\times 10^{-4}$	6.81	6.55	6.93	···	4.28	6.37 ± 5.32	2.45
N $\times 10^{-4}$	1.48	3.77	1.44	1.33	0.63	1.58 ± 1.36	0.64
O $\times 10^{-4}$	2.03	5.34	2.50	3.11	1.42	4.56 ± 2.21	4.74
Ne $\times 10^{-5}$	4.96	11.7	3.79	6.90	6.43	11.2 ± 8.24	7.17
S $\times 10^{-6}$	3.67	6.66	5.42	2.70	2.36	7.55 ± 5.10	14.7
Ar $\times 10^{-6}$	1.16	2.77	1.13	1.60	1.23	2.51 ± 1.98	2.53
Cl $\times 10^{-7}$	0.64	1.52	1.30	0.67	0.88	1.14 ± 0.41	2.49
K $\times 10^{-8}$	3.28	7.83	3.28	···	7.01	···	12.5
Ca $\times 10^{-8}$	3.78	9.00	2.07	···	11.6	···	21.2
Fe $\times 10^{-7}$	2.02	4.70	2.02	···	···	$0.32 - 13.0$	289
Kr $\times 10^{-9}$	6.58	16.7	···	···	···	$5.44\ ^{+4.03}_{-2.32}$	1.91

compiled by Lodders (2003) and Asplund, Grevesse, & Sauval (2005).

Differences between our Std set of abundances and those found by KHM amount to less than ∼35% and are not systematic. On the contrary, there are large discrepancies with most of the abundances reported by H94. Our carbon, nitrogen, oxygen and sulfur abundances are 1.6, 2.3, 1.4 and 1.6 times larger, whereas K and Ca are less than half as large. A plausible interpretation is that entirely different regions are being sampled, since our aperture is much larger and it includes all the inner region of IC 2165. This may explain why we compute much smaller concentrations for K^{+3} and Ca^{+4} than H94, though the assumed temperatures are very similar and our ICFs are much larger. If H94 is pointing to a region where the excitation conditions are well above the mean, the abundances of potassium and calcium reported by H94 are probably excessive. On the other hand, there are important differences on the data used in both works. For instance, H94 adds up the concentrations of C^{+}, C^{+2} and C^{+4}, but overlooks C^{+3}. In the case of nitrogen, H94 uses IUE data to add the concentrations of practically all nitrogen ions, whereas we only have N^{+} to project the abundance of nitrogen from a ICF. In the case of sulfur, we rely on a ICF to account for unobserved ions, whereas H94 includes the concentration of S^{+3} using a measurement of the intensity of [S IV]10.5 μm from an undisclosed source.

As can be seen in Table 4, both abundance sets (Std and 2C) indicate that IC 2165 is a non-type I PN, the end product of a ZAMS progenitor with a mass equal to or less than ∼2 $M_{\odot}$, as had been established by Quireza et al. (2007). From this table we also conclude that the abundance of iron in IC 2165 is near the middle of the range of the iron abundances determined by Delgado-Inglada et al. (2009) for 24 Galactic PNe. A comparison with the mean solar abundance (Lodders 2003; Asplund et al. 2005) suggests that iron, and calcium to a lesser extent, is almost fully depleted into grains. Finally, the Std abundance of krypton in IC 2165 is very close to the mean value found in 10 bright PNe and substantially larger than the solar abundance. This implies that in IC 2165, krypton was produced by slow neutron capture nucleosynthesis during the third dredge up process of the central star (Sterling et al. 2007), a process that is only possible for stellar progenitors having a zero-age main sequence mass larger than ∼1.2 $M_{\odot}$. On the other hand, Sterling & Dinerstein (2008) find that type I PNe exhibit little or no s-process enrichments. Thus, the chemistry of IC 2165 indicates that the zero age main sequence mass of the progenitor star was between ∼1.2 and 2 $M_{\odot}$

3.3. *Nebular mass*

The ionized hydrogen mass can be estimated from

$$M(\mathrm{H}^{+}) = \frac{4\pi D^2 I(\mathrm{H}\beta) m_{\mathrm{H}}}{\langle N_e \rangle \mathrm{E}_{42}}\,, \qquad (4)$$

where D is the distance to the object, $I(\mathrm{H}\beta)$ is the Hβ flux corrected for reddening, m_{H} is the proton mass, $\langle N_e \rangle$ is the mean electron density and E_{42} is the effective recombination emissivity of the Hβ

line. At a distance of 2.53 kpc, the ionized hydrogen mass is equal to 0.06 $M_\odot$ (0.08 including helium) if the mean temperature and density are 13600°K and 4100 cm^{-3}. If there is a cold component and $T(H^+)$ = 5000°K, the ionized hydrogen mass is 0.02 $M_\odot$ (0.03 including helium), assuming pressure equilibrium between the hot and cold components.

4. PHOTOIONIZATION MODEL

The spectrum of IC 2165 was re-analyzed using version 10.00 of the CLOUDY photoionization code (Ferland et al. 1998) with it's default optimization method (Subplex; Rowan 1990). Photoionization models assume equilibrium conditions, which implies that the smallest timescales must be associated to atomic processess.

The incident continuum is produced by a halo abundance He-Ni model photosphere for central stars of planetary nebulae (Rauch 2003). Stellar temperature and luminosity, T_* and L_*, were left as free parameters. Solar abundance models can reproduce the observed spectrum with almost the same accuracy, but require a stellar luminosity and temperature that do not match any theoretical evolutionary track of PN nuclei (Vassiliadis & Wood 1994; Blöcker 1995). Stellar gravity, g_*, was assumed to be equal to 10^6 cm s^{-2}. Rauch models do not include mass loss, which can alter the ionizing flux from the central star (Kudritzki & Puls 2000).

The model nebula is a static sphere surrounding the central star and letting no inward-directed diffuse line or continuum radiation escape, which implies that the covering and filling factors are equal to one. The default cosmic ray background was included. Grain abundance was assumed to be uniform and equal to CLOUDY's standard value. The AGB grain set was used in this model and photoelectric heating was considered.

The best results were obtained assuming that $N_{\rm H} \propto R^{-2}$, where R is the distance to the exciting star and $N_{\rm H}$ is the total hydrogen density. Notice that this density law is consistent with a constant mass loss rate. The inner radius and the total hydrogen density at this point, were left as free parameters.

The abundances of helium, carbon, nitrogen, oxygen and neon were free parameters in each model run. Sulfur, argon, chlorine, potassium, calcium and iron abundances, were modified from run to run since these elements are not important cooling agents. Abundances for other elements are taken from CLOUDY's PN set and were kept fixed. Considering their small importance in the structure of photoionized regions, lithium, beryllium, boron, scandium, titanium, vanadium, chromium, manganese, cobalt, copper and zinc were not included.

TABLE 5

MODEL PARAMETERS

$L_*/L_\odot$	8766	He	0.106
T_* °K	130699	C $\times10^{-4}$	6.93
log g_* cm s^{-2}	6.0	N $\times10^{-4}$	1.44
R(in) 10^{17} cm	0.782	O $\times10^{-4}$	2.50
$N_{\rm H}$(in) cm^{-3}	19380	Ne $\times10^{-5}$	3.79
N_e(in) cm^{-3}	23500	S $\times10^{-6}$	5.42
T(in) °K	18820	Ar $\times10^{-6}$	1.13
R(out) 10^{17} cm	2.762	Cl $\times10^{-7}$	1.30
$N_{\rm H}$(out) cm^{-3}	1545	K $\times10^{-8}$	3.28
N_e(out) cm^{-3}	1586	Ca $\times10^{-8}$	2.07
T(out) °K	12420	Fe $\times10^{-7}$	2.02
log $L(H\beta)$ erg s^{-1}	35.21		

Model runs were set to optimize the intensities of [O II] 3726,3729 Å, [Ne III] 3869 Å, C II 4267 Å, He II 4686 Å, [Ar IV] 4711,4740 Å, He I 5876 Å, [O III] 4363,5007 Å and [N II] 5755,6584 Å with respect to Hβ. Calculations stop when [S II] 4069/Hβ reaches the observed value. This stopping criterion underestimates the intensity of the nitrogen and oxygen neutral lines, but produced much better results than models where calculations were over once [O I]6300/Hβ reached the observed value, in which case all neutral lines were accurately reproduced. This indicates that there is a significant amount of neutral material beyond the outer edge of the inner nebula.

Values for the luminosity, effective temperature and gravity of the central star of the best photoionization model, as well as the inner and outer radius, R(in) and R(out), total hydrogen density, $N_{\rm H}$(in) and $N_{\rm H}$(out), electron density, N_e(in) and N_e(out), electron temperature, T(in) and T(out), and abundances of the model nebula, are presented in Table 5. The stellar temperature and luminosity imply that the radius and mass of an equivalent black body are 0.18 $R_\odot$ and 1.24 $M_\odot$.

Model abundances confirm that IC 2165 is a non-type I PNe. The abundances of helium, carbon, nitrogen, oxygen, argon and iron are similar to those derived using ICFs and the standard approach. The model neon abundance is 25% smaller, since the neon to oxygen abundance ratio is smaller than Ne^{+2}/O^{+2} in the photoionization model, and not equal to it

as is assumed in the ICF. Since [K IV] 6102 Å is not calculated in the photoionization model and, as far as we know, krypton is not considered in version 10.00 of the CLOUDY code, the model assumed the abundances of potassium and krypton that were determined in § 3.2.

Chlorine and sulfur abundances are 2.4 and 1.8 times larger in the model than those found from ICFs and the standard approach, whereas calcium model abundance is 1.8 times smaller. These discrepancies do not seem to be related to inadequate ICFs. For instance, we assumed that the sum of Cl^{+2} and Cl^{+3} is nearly equal to the abundance of chlorine. The photoionization model supports this assumption: 97% of chlorine is as Cl^{+2} and Cl^{+3}. In the case of sulfur, model results show that the concentration of unobserved sulfur ions, particularly S^{+3}, is adequately taken into account by the ICF. And the model successfully replicates the relative intensity of [Ca V] 5309 Å and the ICF defined in equation 2, i.e., $Ca^{+4}/Ca = Ar^{+4}/Ar$. These inconsistencies are probably related to differences in some atomic parameters used in IRAF's IONIC and TEMDEN tasks and CLOUDY 10.00. For instance, in the case of S II and S III, the IRAF tasks use transition probabilities from various authors (Mendoza & Zeippen 1982; Kaufman & Sugar 1986; LaJohn & Luke 1993; Keenan et al. 1993; Heise, Smith, & Calamai 1995; Verner, Verner, & Ferland 1996), whereas CLOUDY 10.0 relies entirely on those calculated by Podobedova, Kelleher, & Wiese (2009). These codes also use different sources for the transition probabilities of the chlorine and calcium ions, as well as the collision strengths of Cl III.

Line intensities for the best modeled spectrum are presented in Table 1 under the column labeled as $I_{\rm mod}$. For the 12 lines used to optimize the model, the mean difference between observed and modeled values is 6%. For the 75 lines that were modeled, the mean difference is 27%. Measurement errors probably account for most individual differences larger than 50%, since these are mostly found in weak lines with no more than two measurements, such as H 13, [Fe III] 4702 and [Cl IV] 5323 Å. On the other hand, the model underestimates nitrogen and oxygen neutral lines (for [O I] 5577 Å, bad sky subtraction accounts for the huge difference). Neutral lines are successfully reproduced using [O I] 6300/Hβ as the stopping criterion, but the relative intensities of the 12 lines used to optimize the model run are less accurate and the external temperature and electron density are much smaller (T(out) $\simeq$ 4000°K and N_e(out) $\simeq$ 50 cm^{-3}).

With the 60 lines where model intensities differ less than 50%, the mean difference between observed and modeled intensities is 14%. The two temperature dependent line ratios are nearly identical to the observed ratios: [N II](6548+6584)/5755 = 48.18 vs. 51.27 and [O III](4959+5007)/4363 = 81.68 vs. 80.72 (model values first). Agreement between electron density sensitive line ratios is fairly reasonable, but not as good: [Ar IV]4711/4740 = 0.64 vs. 0.83, [Cl III]5518/5538 = 0.83 vs. 0.82, [O II]3726/3729 = 1.50 vs. 1.67 and [N I]5198/5200 = 1.40 vs. 1.52. The model prescribes a slightly steeper electron density distribution, that is, a larger density for the Ar^{+3} line ratio, a similar one for the Cl^{+2} ratio and smaller densities for the the O^{+} and N^{0} line ratios. Overall, the photoionization model is a fairly good approximation to the observed spectrum, insofar as relative line intensities and temperature and density sensitive line ratios are considered.

From R(out) and the nebular diameter at the 10% level of peak surface brightness of the Hα+[N II] (6548+6584) image, which is $9\farcs0 \times 8\farcs9$ (Tylenda et al. 2003), the photoionization model implies that the distance to IC 2165 is 4.1 kpc, slightly larger than the largest distance estimate (3.9 kpc, Tajitsu & Tamura 1998). Given the intrinsic Hβ luminosity, L(Hβ), at this distance the Hβ line intensity of the photoionization model is 8.0×10^{-11} erg cm^{-2} s^{-1}, 2.5 times larger than the observed intensity. Thus, the model does not replicate these two global properties.

From the outer radius of the model and the expansion velocity of the nebula, 25 km s^{-1} according to Acker et al. (2002), the dynamical age of the PN model turns out to be close to 3500 year, substantially larger than the longest atomic timescale in the photoionization model (112 yr). Taking into account that $N_{\rm H} \propto R^{-2}$, we can easily find that the total nebular mass in the photoionization model is 0.35 $M_\odot$, about four times larger than our previous estimate for the ionized gas mass which, among other things, was based on the assumption that IC 2165 is 1.6 times closer than the distance implied by the photoionization model (see § 3.3).

The mass of the zero-age main sequence progenitor can be estimated finding which theoretical evolutionary tracks for the effective temperature and luminosity of PN nuclei are closest to the exciting star in an HR diagram. As can be seen from Figure 2, two tracks produced by Vassiliadis & Wood (1994) compare very favorably with the luminosity and temperature predicted by our photoionization model. One of them is for a 2.0 $M_\odot$ zero-age main sequence star

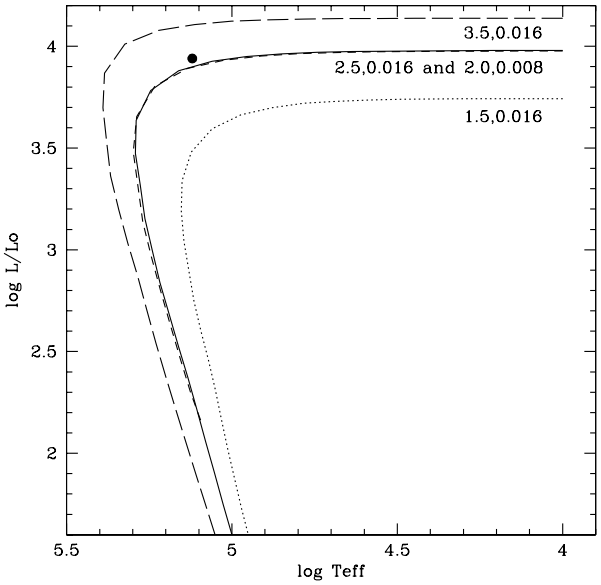

Fig. 2. Vassiliadis & Wood (1994) evolutionary tracks for H burning shell PN nuclei produced by 1.5, 2.5 and 3.5 $M_\odot$ zero-age main sequence stars with metallicity $Z = 0.016$ and by a 2.0 $M_\odot$ main sequence star with $Z = 0.008$, as labeled in the figure. The position of the central star of the photoionization model is marked with a dot. It is very close to the evolutionary tracks of a 2.5 $M_\odot$ zero-age main sequence star where $Z = 0.016$ (solid) and a 2.0 $M_\odot$ zero-age main sequence star where $Z = 0.008$ (dashed). The tracks start at the upper-right hand corner.

with $Z = 0.008$, where the effective temperature of the H burning shell has been larger than 10^4°K for ∼2000 yr (this is the way age is measured in these models). The second one is a ∼1600 yr old H burning shell PN nucleus produced by a 2.5 $M_\odot$ zero-age main sequence star where $Z = 0.016$. No other evolutionary track can do this. This is consistent with all the other evidence indicating that the zero-age main sequence mass of the precursor was close to 2 $M_\odot$.

5. CONCLUSIONS

From open slit high dispersion Echelle observations of the entire ∼10″ inner region of planetary nebula IC 2165, we find that the best fit between observed and theoretical Balmer line ratios is when $C(\mathrm{H}\beta)$=0.39 and $T(\mathrm{H}^+)$=5000°K. Thus, the existence of two nebular components characterized by very different temperatures is a distinct possibility.

Temperature and density sensitive forbidden line ratios imply that the object has a relatively uniform and high electron temperature, higher than ∼13000°K, and electron densities that are much larger in the highly excited regions that face the PN nucleus. Thus, thermal pressure contributes to nebular expansion.

Abundances based on ICFs were calculated from forbidden lines using the standard approach (Std), the same temperature for H^+ and the ion, as well as assuming that recombination lines are produced in a medium where the characteristic temperature is 5000°K (a two component approach, 2C). As expected, the 2C approach leads to larger abundances. Nevertheless, the two sets of abundances imply that IC 2165 is a non-type I PN, as has been argued before. Additionally, the large abundance of krypton (as with K and Ca, derived from our own ICF) is at least 2.5 times higher than the solar value, which indicates that s-process nucleosynthesis was very effective in IC 2165, a process that can only take place in stars more massive than ∼1.2 $M_\odot$ but smaller than ∼2.0 $M_\odot$ when in the main sequence (Sterling et al. 2007; Sterling & Dinerstein 2008).

Calcium abundance is at least two times smaller than the solar value, whereas iron may be more than 200 times less abundant than in the Sun. Thus, in IC 2165 these two elements have been heavily depleted into grains.

Assuming that IC 2165 is 2.53 kpc away and has a mean electron density of 4100 cm^{-3}, we estimate that the ionized gas mass of the inner nebula, which may be the latest eruption of the central star, is between ∼0.08 (Std approach) and 0.03 $M_\odot$ (2C approach).

The spectrum was fairly well replicated by a photoionization model produced with version 10.00 of the Cloudy code (Ferland et al. 1998). Calculations stop when [S II] 4069/Hβ reaches the observed value. Among other things, we assume an inverse square law for the hydrogen nebular density and a halo abundance He-Ni Rauch (2003) photosphere for the exciting source. The mean difference between 75 modeled and observed lines is 27%. Excluding lines that were poorly measured and lines from neutral species that probably lie beyond the outer edge of the inner nebula, the mean difference for the remaining 60 lines is 14%. All electron density and temperature sensitive line ratios are satisfactorily reproduced.

Most model abundances are quite similar to those derived using the simple well known recipes that define the standard approach. Not so for sulfur, chlorine and calcium, where we found that the ICFs were adequate. In these cases the discrepancy may be related to differences in atomic parameters contained in Cloudy 10.00 and those used in IRAF's temden

and IONIC tasks. Model abundances also imply that IC 2165 is a non-type I PN.

The model cannot account for some global properties. For instance, the model outer radius and angular size of the inner nebula imply a distance of 4.1 kpc to IC 2165, 10% more than the largest distance estimate. At this distance, the Hβ line intensity of the photoionization model would be 2.5 times larger than the observed value. We also find that the total nebular mass of the photoionization model is four times larger than the observational estimate for the mass of ionized gas, where we assumed that the distance was 1.6 times smaller than the one implied by the model.

Finally, the effective temperature and luminosity of the central star are very close to two evolutionary tracks of PN nuclei (Vassiliadis & Wood 1994). One of these is for a 2.5 $M_{\odot}$ zero-age main sequence progenitor with $Z = 0.016$. The second alternative is consistent with many other lines of evidence, since it is for a 2.0 $M_{\odot}$ progenitor with $Z = 0.008$. Consequently, all evidence indicates that IC 2165 was produced by a metal poor 2 $M_{\odot}$ A5 V star that took off some 2×10^9 yr ago.

Comments from an anonymous referee and the assistance of the San Pedro Mártir Observatory staff are gratefully acknowledged. J.B. acknowledges support from PAPIIT/Universidad Nacional Autónoma de México grant IN-101813. M.R. acknowledges support from Mexican Conacyt grant CB-2009-01/131620.

REFERENCES

Acker, A., Gesicki, K., Grosdidier, Y., & Durand, S. 2002, A&A, 384, 620
Acker, A., & Neiner, C. 2003, A&A, 403, 659
Aller, L. H. 1984, Physics of Thermal Gaseous Nebula (Dordrecht: Reidel)
Asplund, M., Grevesse, N., & Suval, A. J. 2005, in ASP Conf. Ser. 336, Cosmic Abundances as Records of Stellar Evolution and Nucleosynthesis, ed. Thomas G. Barnes III & Frank N. Bash (San Francisco: ASP), 25
Ballance, C. P., Griffin, D. C., & McLaughlin, B. M. 2007, J. Phys. B: At. Mol. Opt. Phys., 40, 327
Biémont, E., & Hansen, J. E. 1986, Phys. Scr., 33, 117
Blöcker, T. 1995, A&A, 299, 755
Bohigas, J. 2008, ApJ, 674, 954
Cahn, J. H., Kaler, J. B., & Stanghellini, L. 1992, A&AS, 94, 399
Campbell, W. W., & Moore, J. H. 1918, Pub. Lick Obs., 13, 75
Chen, G. X., & Pradhan, A. K. 1999, A&AS, 136, 395
_____. 2000, A&AS, 147, 111
Corradi, R. L. M., Schönberner, D., Steffen, M., & Perinotto, M. 2003, MNRAS, 340, 417
Daub, C. T. 1982, ApJ, 260, 612
Davey, A. R., Storey, P. J., & Kisielius, R. 2000, A&AS, 142, 85
Delgado-Inglada, G., Rodríguez, M., Mampaso, A., & Viironen, K. 2009, ApJ, 694, 1335
Ferland, G. J., Korista, K. T. Verner, D. A., Ferguson, J. W., Kingdon, J. B., & Verner, E. M. 1998, PASP, 110, 761
Grandi, S. A. 1976, ApJ, 206, 658
Gutiérrez-Moreno, A., Moreno, H., & Cortés, G. 1985, PASP, 97, 397 (GMC)
Heap, S. R., Corcoran, M., Hintzen, P., & Smith, E. 1990, in From Miras to Planetary Nebulae: Which Path for Stellar Evolution, ed. M. O. Menessier & A. Omont (France: Editions Frontières), 397
Heise, C., Smith, P. L., & Calamai, A. G. 1995, ApJ, 451, L41
Henry, R. B. C., Kwitter, K. B., & Bates, J. A. 2000, ApJ, 531, 928
Hyung, S. 1994, ApJS, 90, 119 (H94)
Kaufman, V., & Sugar, J. 1986, J. Phys. Chem. Ref. Data, 15, 321
Keenan, F. P., Hibbert, A., Ojha, P. C., & Conlon, E. S. 1993, Phys. Scr., 48, 129
Kingdon, J., & Ferland, G. J. 1995, ApJ, 442, 714
Kingsburgh, R., & Barlow, M. J. 1994, MNRAS, 271, 257
Kudritzki, R.-P., & Puls, J. 2000, ARA&A, 38, 613
Kwitter, K. B., Henry, R. B. C., & Milingo, J. B. 2003, PASP, 115, 80 (KHM)
LaJohn, L., & Luke, T. M. 1993, Phys. Scr., 47, 542
Lodders, K. 2003, ApJ, 591, 1220
Maciel, W. J. 1984, A&AS, 55, 253
Mendoza, C., & Zeippen, C. J. 1982, MNRAS, 199, 1025
Mihalas, D., & Binney, J. 1981, Galactic Astronomy: Structure and Kinematics (San Francisco: Freeman)
Nahar, S. N., Delahaye, F., Pradhan, A. K., & Zeippen, C. J. 2000, A&AS, 144, 141
Peimbert, M., Luridiana, V., & Torres-Peimbert, S. 1995, RevMexAA, 31, 147
Péquignot, D., Petitjean, P., & Boisson, C. 1991, A&A, 251, 680
Phillips, J. P. 2004, MNRAS, 353, 589
Podobedova, L. I., Kelleher, D. E., & Wiese, W. L. 2009, J. Phys. Chem. Ref. Data, 38, 171
Pottasch, S. R., Bernard-Salas, J., Beintema, D. A., & Feibelman, W. A. 2004, A&A, 423, 593
Quinet, P. 1996, A&AS, 116, 573
Quireza, C., Rocha-Pinto, H. J., & Maciel, W. J. 2007, A&A, 475, 217
Rauch, T. 2003, A&A, 403, 709
Rowan, T. 1990, PhD Thesis, The University of Texas, USA
Schöning, T. 1997, A&AS, 122, 277
Seaton, M. J. 1979, MNRAS, 187, 73P

Shaw, R. A., & Dufour, R. 1994, in ASP Conf. Ser. 61, Astronomical Data Analysis Software and Systems III, ed. D. R. Crabtree, R. J. Hanisch, & J. Barnes (San Francisco: ASP), 327
Stanghellini, L., Shaw, R. A., & Villaver, E. 2008, ApJ, 689, 194
Sterling, N. C., & Dinerstein, H. L. 2008, ApJS, 174, 158
Sterling, N. C., Dinerstein, H. L., & Kallman, T. R. 2007, ApJS, 169, 37
Storey, P. J. 1994, A&A, 282, 999
Storey, P. J., & Hummer, D. G. 1995, MNRAS, 272, 41
Tajitsu, A., & Tamura, S. 1998, AJ, 115, 1989
Tylenda, R., Siódmiak, N., Górny, S. K., Corradi, R. L. M., & Schwarz, H. E. 2003, A&A, 405, 627
Van de Steene, G. C., & Zijlstra, A. A. 1994, A&AS, 108, 485
Vassiliadis, E., & Wood, P. R. 1994, ApJS, 92, 125
Verner, D. A., Verner, E. M., & Ferland, G. 1996, At. Data Nucl. Data Tables, 64, 1
Verner, E. M., Verner, D. A., Baldwin, J. A., Ferland, G. J., & Martin, P. G. 2000, ApJ, 543, 831
Witthoeft, M. C., & Badnell, N. R. 2008, A&A, 481, 543
Wilson, O. C. 1950, ApJ, 111, 279
Wolff, M. J., Code, A. D., & Groth, E. J. 2000, AJ, 119, 302
Zhang, C. Y. 1995, ApJS, 98, 659
Zhang, H. 1996, A&AS, 119, 523

Joaquín Bohigas: Instituto de Astronomía, Universidad Nacional Autónoma de México, Km. 103 Carretera Tijuana-Ensenada, 22860 Ensenada, B. C., Mexico (jbb@astrosen.unam.mx).
Reginald James Dufour: Physics and Astronomy Department, Rice University, 6100 Main MS-61, Houston, Texas 77005-1827, E.U.A. (rjd@rice.edu).
Mónica Rodríguez: Instituto Nacional de Astrofísica, Óptica y Electrónica (INAOE), Apdo. Postal 51 y 216, 72000 Puebla, Mexico (mrodri@inaoep.mx).